ISSN: 2993-6594

Research Article

Open Access Journal of Disease and Global Health

Analysis of the Impact of Emissivity and Albedo on Urban Mean Radiative Temperature

Abdelilah Zyane* and Herve Pron

University of Reims Champagne Ardenne URCA, Institut de Thermique, Mécanique et Matériaux, EA 7548 / Equipe Thermique – Energétique Campus du Moulin de la Housse, France

***Corresponding Author**
Abdelilah Zyane, University of Reims Champagne Ardenne URCA Institut de Thermique, Mécanique et Matériaux, EA 7548 / Equipe Thermique – Energétique Campus du Moulin de la Housse, France.

Submitted: 2025, Aug 13; **Accepted:** 2025, Dec 16; **Published:** 2026, Feb 26

Citation: Zyane, A., Pron, H. (2026). Analysis of the Impact of Emissivity and Albedo on Urban Mean Radiative Temperature. *Ope Acce Jou Dis Glo Heal, 4*(1), 01-16.

Abstract

As part of efforts to promote energy-climate planning solutions and develop governance support platforms and tools, the issue of urban heat islands (UHIs) significantly impacts on urban thermal comfort, energy balance parameters, and ultimately, the mitigation of greenhouse gas (GHG) emissions. This article aims to investigate the influence of radiative emissivity and albedo on UHIs, and consequently, on thermal comfort indicators, urban energy balances, and their contribution to climate change at the urban scale.

An in-depth analysis of radiative emissivity and albedo parameters is conducted to assess their effects on the mean urban radiative temperature.

Based on the adopted scientific methodology, the article proposes recommendations and insights to support energy-climate planning strategies to facilitate the urban energy transition.

Keywords: Urban Heat Island, Urban Dynamic Thermal Simulation, Urban Energy Transition, Energy-Climate Planning, Climate Change.

1. Introduction

The energy transition is a critical challenge for ensuring a sustainable future. Therefore, promoting solutions to reduce the effects of global warming at the urban scale is essential. According to the Intergovernmental Panel on Climate Change (IPCC) forecasts, global temperatures have already increased by 1.5°C compared to pre-industrial levels, along with corresponding trajectories of rising greenhouse gas emissions [1].

The rate of urbanization continues to rise, with the global population projected to reach 10 billion by 2050, 68% of whom are expected to live in urban areas [2]. This rapid urban expansion significantly influences microclimatic phenomena, increasingly contributing to temperature rises in local climate zones [3]. Consequently, surface and air temperatures increase, while convective heat exchange decreases, negatively affecting urban energy balances.

Changes in radiative parameters—specifically albedo and radiative emissivity—further influence the mean radiative temperature, thereby affecting outdoor thermal comfort. The deterioration of urban thermal comfort poses health risks to inhabitants, leads to intensified surface heating, increases cooling energy demand, and complicates efforts to reduce greenhouse gas emissions [4].

Urban morphology plays a crucial role in determining radiative parameters, particularly albedo and emissivity. Its influence is expressed through several factors, including shading effects, complex three-dimensional reflections between urban surfaces, and the physical properties of construction materials. Urban morphology has been re-examined from a new perspective to address existing gaps in the understanding of its morphological characteristics [5].

The albedo of the urban canopy—which comprises various horizontal and vertical exchange surfaces—is a fundamental parameter in evaluating radiative heat fluxes exchanged with the atmosphere. A study conducted across several European cities demonstrated that the intensity of the urban canopy heat island

(UHI) effect can reach up to 10°C within cities [6].

The impact of optimizing urban typology and design on heat islands was explored by (Shayan Mirzabeigi and Mohamad Razkenari 2022), highlighting how urban geometry, morphological parameters, and building envelope characteristics influence both energy efficiency and outdoor thermal comfort, thereby affecting climate change [7]. Their study proposes an optimization framework using Grasshopper plug-ins such as Ladybug and Eddy3D to generate optimal design scenarios. Other studies have also considered energy infrastructure, spatial characteristics, and additional morphological aspects [8].

The spatio-temporal analysis of external comfort temperature (ECT) in relation to urban heat islands, as explored in the study by (Reihaneh Aghamolaei, Marzieh Fallahpour, and Parham A. Mirzaei (2021), presents a series of simulations aimed at optimizing ECT under varying solar radiation and wind speed scenarios [9]. The study concluded that ECT varies significantly with spatio-temporal factors. Airflow has a more pronounced effect in the morning and is less impactful in the afternoon. Additionally, the Physiological Equivalent Temperature (PET) was found to fluctuate considerably near the edges and boundaries of buildings, where airspeed tends to be higher.

The study conducted by L. Mariani, S.G. Parisi, G. Cola, R. Lafortezza, G. Colangelo, and G. Sanesi (2016) on the climatic effects of vegetation in mitigating urban heat islands clearly demonstrated that enhancing and optimizing specific components of park structures can significantly improve the urban cooling effect [10].

Conversely, the impact of urban thermal inertia on heat islands underscores the critical importance of measuring and analyzing the various contributing factors. Heat generated by human activities, combined with circulation dynamics within urban areas, plays a significant role in shaping thermal behavior. The analysis of local effective thermal inertia carried out by Masanori Onishi, Isao Iizawa, Miki Fukuzawa, Satoshi Sakai, Kazuhiro Umetani, Aya Ito, Arata Yajima, Kosaku Ono, and Naoki Amemura (2007) highlights that urban areas possess considerably higher thermal properties than rural environments, thereby increasing the complexity of mitigating the urban heat island effect [11].

Albedo is a key parameter that reflects a surface's ability to reflect solar radiation, thereby indicating the proportion of radiation absorbed. It varies significantly across the different spectral bands of solar radiation—ultraviolet (UV), visible, and near-infrared. A white surface, with an albedo close to 1, reflects nearly all incoming solar radiation and contributes to surface cooling, whereas a black surface, with an albedo near 0, absorbs almost all radiation and contributes to surface warming. In the near-infrared range, albedo is influenced by additional factors, particularly the nature and properties of the surface. For instance, coniferous forests exhibit a very low albedo (~0.09), making them less reflective than other types of vegetation such as grasslands, which typically range from 0.14 to 0.165.

In parallel, while various urban materials absorb solar radiation within the visible spectrum and reemit energy in the infrared, emissivity becomes especially relevant in the thermal infrared range. This is particularly true within the two principal atmospheric windows: 3–5 µm, associated with high temperatures, and 8–14 µm, which corresponds to ambient temperature conditions.

This article presents a detailed analysis of the influence of albedo and emissivity on urban heat islands, with a specific focus on their effects on mean radiative temperature. Several simulation scenarios were developed to identify optimal values for these radiative parameters, aiming to minimize the negative impacts associated with materials commonly used in urban infrastructure and to enhance thermal comfort at the urban scale.

2. Methodology

The framework developed in this study proposes a step-by-step methodology to optimize the albedo and radiative emissivity of urban surfaces, considering the diverse material properties present in the built environment. This approach is based on a dynamic thermal simulation of mean radiative temperature, using the UMEP-SOLWEIG model integrated within QGIS. The computational model was applied to the city of Reims, with spatial data acquired through LIDAR technology.

The analysis framework consists of three main stages, as illustrated in Figure 1. The first stage involves the mapping of 2D and 3D spatial geometry through the extraction of raw geospatial data. The second stage focuses on the development of a comprehensive database of material properties, integration of meteorological data, and satellite-derived observations of albedo and emissivity values to construct relevant simulation scenarios. The third and final stage entails the simulation of mean radiative temperature using the UMEP-SOLWEIG tool within QGIS. This enables the evaluation of thermal comfort conditions at the urban scale and the subsequent assessment of the urban heat island effect.

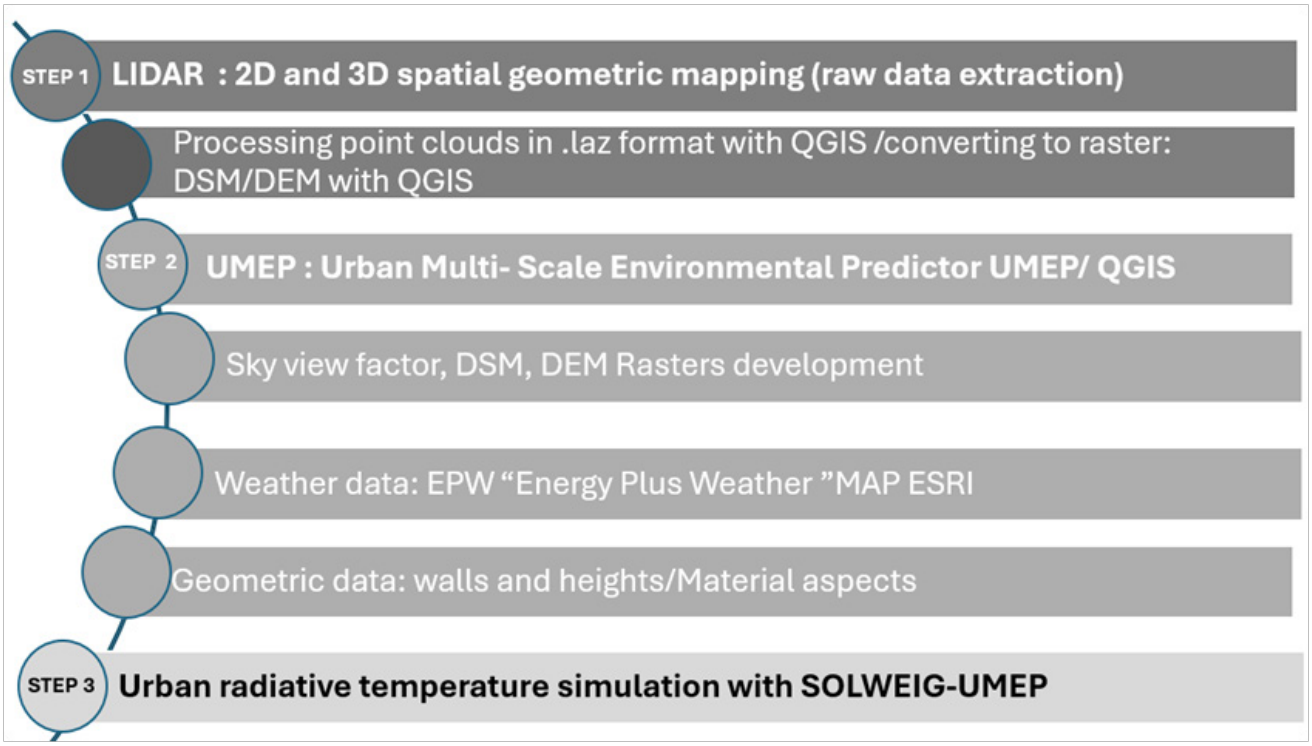

Figure 1: Urban radiative temperature simulation steps Study zone: City of Reims, France

Reims is a commune located in the Marne department (department 51), in Champagne-Ardenne region of northeastern France. As of 2020, the city had an estimated population of approximately 185,034 residents, compared to 183,113 in 2016. With a total area of 49.41 km², this corresponds to a population density of around 3,745 inhabitants per square kilometer.

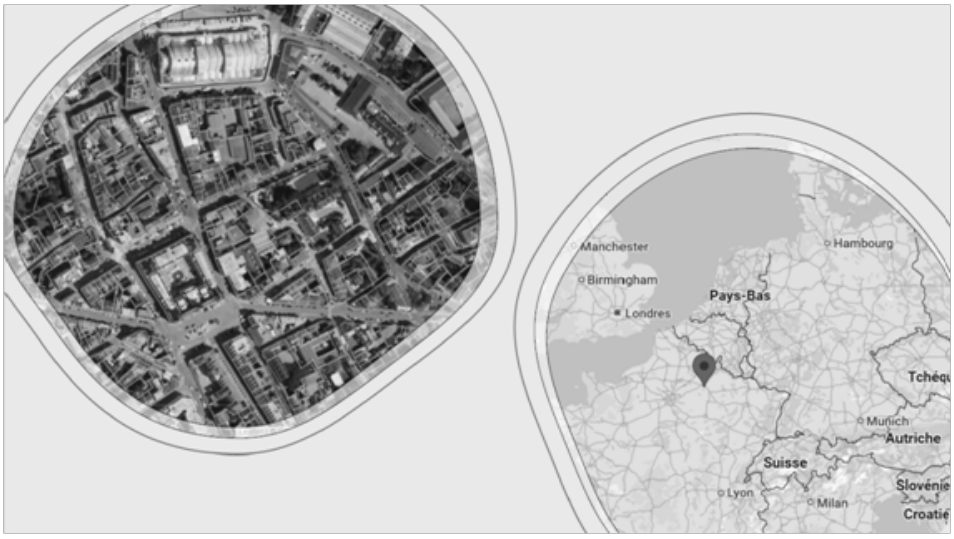

Figure 2: Geographical Location of the City of Reims France

It has been observed that the temperature in the city of Reims has continuously increased over time, as shown in the figure 3 below. This highlights the importance of focusing on improving urban outdoor thermal comfort by optimizing the mean radiative temperature.

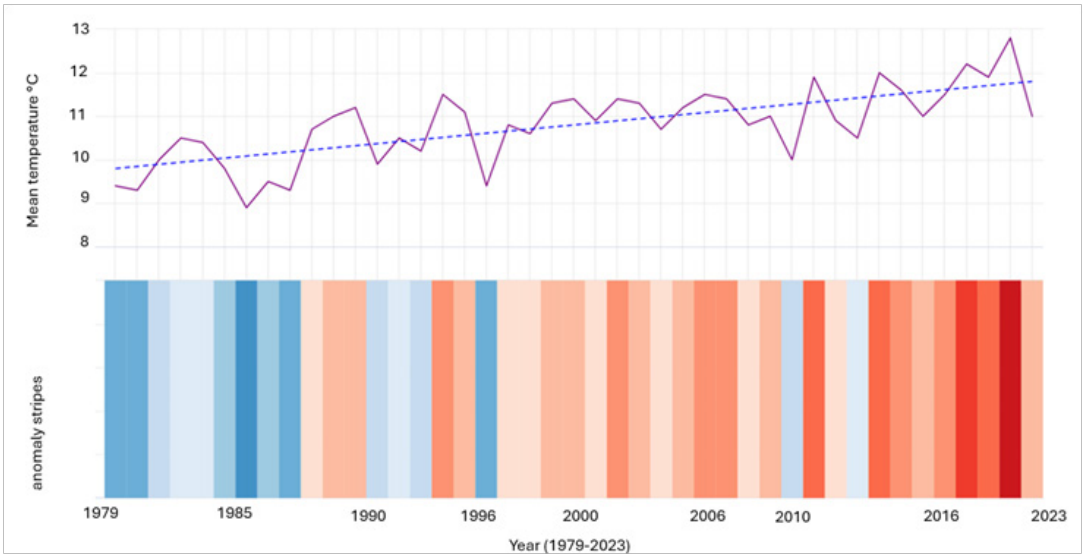

Figure 3: Mean yearly Temperature Evolution in the City of Reims-1979-2023 Source Météo France - Meteoblue

Between 1979 and 2023, the annual mean temperature exhibits a clearly increasing trend, rising from approximately 9.5 °C to over 12.5 °C. Despite some year-to-year variability, the overall curve reflects a continuous warming. This trend is further emphasized by the visualization of "anomaly stripes": colder years (in blue) dominate until the mid-1990s, while recent years—particularly after 2010—are mostly warm (in dark red). The graph thus provides a clear and visual representation of the progression of climate warming over the past four decades.

2.1. Step 1: Data Extraction Using 2D and 3D HD LiDAR Geometric Mapping

LiDAR technology was utilized for terrain mapping and the development of digital elevation models, enabling the generation of high-resolution 3D representations of the city of Reims. These models are essential for conducting radiative thermal analyses of urban heat islands, particularly through the assessment of Mean Radiant Temperature (MRT).

LiDAR—an acronym for Light Detection and Ranging—is an optical remote sensing technique that uses laser pulses to densely scan the Earth's surface, producing highly accurate x, y, and z coordinates. This technology allows for the detailed reconstruction of both terrain and above-ground features.
Source : ArcMap | Documentation (arcgis.com)

As part of the national LiDAR HD program, the French National Institute of Geographic and Forestry Information (IGN) is responsible for producing and disseminating comprehensive 3D mapping of both ground and surface features across France using LiDAR data. The datasets provided include calibrated point clouds (both raw and classified), as well as 3D digital models such as Digital Terrain Models (DTM), Digital Surface Models (DSM), and Digital Height Models (DHM). Sources : LiDAR HD | Géoservices (ign.fr)

For this study, raw LiDAR HD data for the city of Reims was extracted. Each x, y, z point in the dataset contains additional metadata that enriches the spatial analysis. The map below illustrates the various available LiDAR data tiles across France, allowing users to download point clouds corresponding to their area of interest.

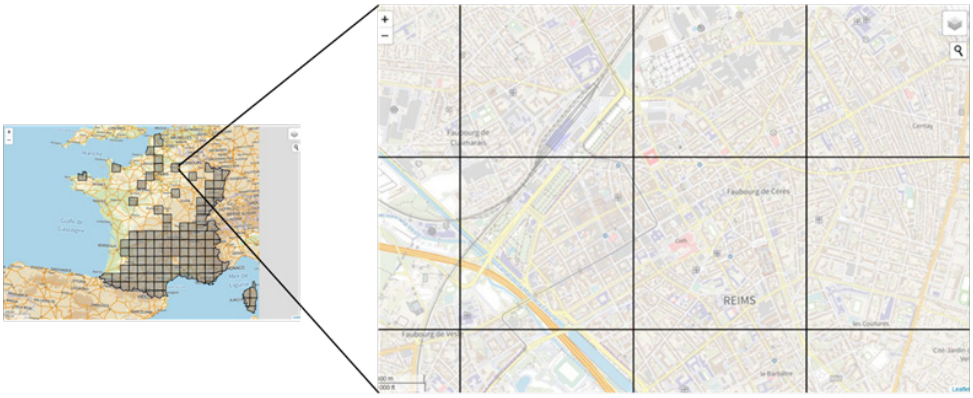

Figure 4: HD LIDAR Data Tiles

The tiles are represented by HD LiDAR point clouds, which are subsequently converted into raster format using QGIS Sources : ArcMap | Documentation (arcgis.com)

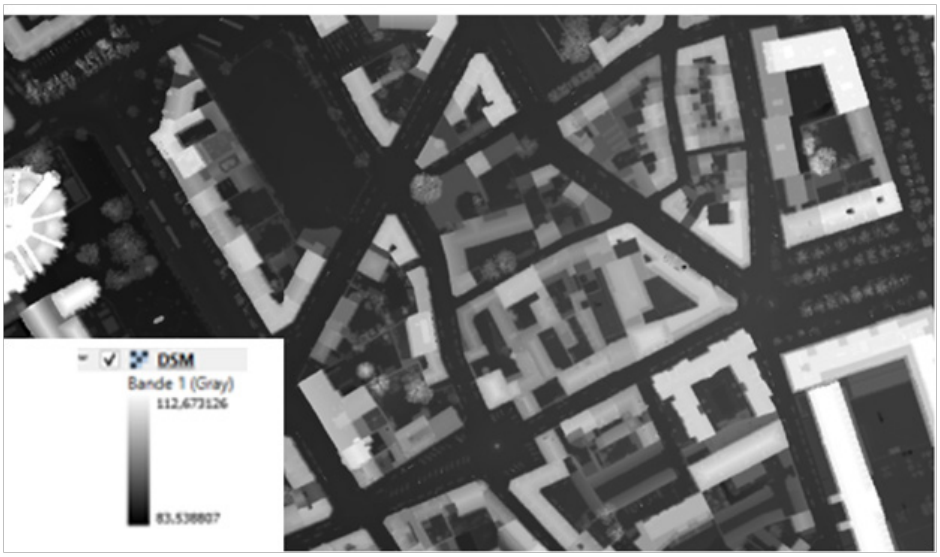

Figure 5: Map Illustrating the Digital Surface Model (DSM) of the Study Area

Raster maps are used to represent various elevation-related geospatial datasets, including the Digital Elevation Model (DEM), Digital Surface Model (DSM), Digital Terrain Model (DTM), and the normalized Digital Surface Model (nDSM). These four components are essential for accurately characterizing urban morphology. Georeferencing within QGIS is a crucial step in aligning raster images to ensure consistency and reliability in subsequent simulations.

The Sky View Factor (SVF) plugin is employed to calculate the SVF for each pixel, based on DSM data that captures both ground and built surfaces. The Sky View Factor is the ratio of radiation received (or emitted) by a flat surface to the radiation that would be received (or emitted) from the entire hemispherical sky dome [12]. It is a dimensionless index ranging from 0 to 1, where 0 represents fully obstructed environments and 1 indicates completely open spaces. The methodology for generating SVF values follows the approach outlined (2010) [13].

The wall height and aspect pre-processor are employed to detect wall pixels and estimate their height using digital surface models (DSMs) of the terrain and built structures. This process involves the application of a filtering technique described [14]. Wall aspect is determined through a specialized linear filter originally proposed [15].

2.2. Step 2: The process entails the retrieval of meteorological data from EnergyPlus Weather (EPW) files, followed by the analysis of surface albedo and emissivity values derived from satellite observations.

Meteorological data from EnergyPlus Weather (EPW) files, combined with satellite-derived datasets provided by the Environmental Systems Research Institute (ESRI), were employed to integrate atmospheric and surface information into the calculation of mean radiant temperature. This integration enables a more accurate representation of radiative thermal dynamics, which is essential for the analysis of urban heat island effects.

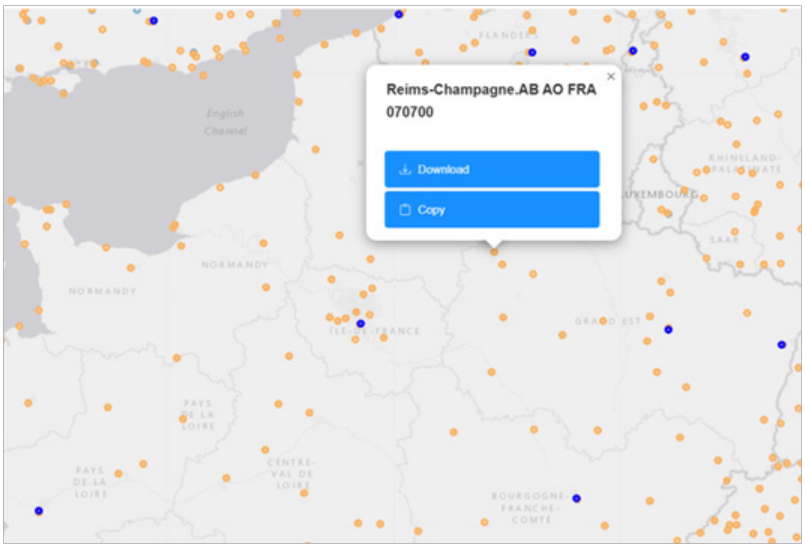

Figure 6: Meteorological Data EPW: source EPW Map (ladybug.tools), with the Various Orange and Blue Dot Stations

The observation and satellite-based modeling of albedo values in the visible and near-infrared spectra will facilitate the identification of these values, which can then be integrated into various optimization scenarios.

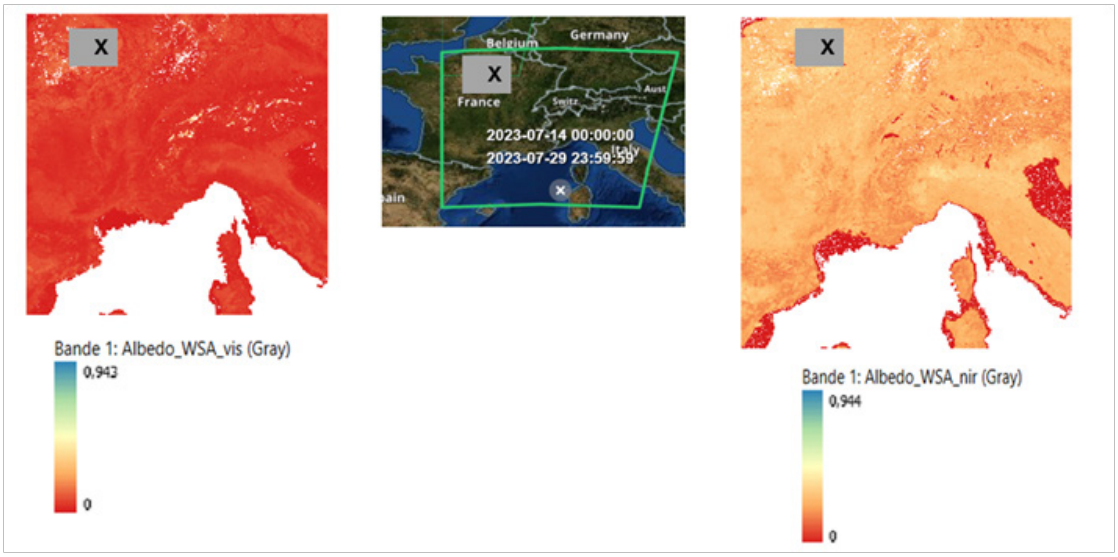

Sources : MODIS/Terra+Aqua BRDF/Albedo Albedo Daily L3 Global - 500m V061 | Earthdata Search (nasa.gov)

Figure 7: Albedo Observation Map WSA « White Sky Albedo » Visible “Vis” on Left Side and Albedo WSA Nir “Near Infrared” in the Right Side

2.3. Step 3: Approach and methodology for simulating mean radiant temperature (MRT) are implemented using UMEP (Urban Multi-scale Environmental Predictor) and the SOLWEIG (Solar and Long Wave Environmental Irradiance Geometry) model.

UMEP is an extension module for QGIS, a Geographic Information System (GIS) software, which enhanced by UMEP, enables advanced geospatial analysis. This integration is particularly useful for studying outdoor thermal comfort, urban energy consumption, and climate change mitigation.

SOLWEIG is employed to estimate spatial variations in 3D radiation fluxes and mean radiant temperature (MRT). Shortwave and longwave radiation fluxes from six directions are calculated separately to derive the MRT. The model requires a limited set of inputs, including direct, diffuse, and global shortwave radiation, air temperature, relative humidity, urban geometry, and geographical data (latitude, longitude, and altitude). Additionally, information on vegetation and its cover is incorporated to improve the estimation of MRT.

The calculation method utilizes longwave sky irradiation as

isotropic, estimating it from sky view factors (SVF) and global emissivity [16]. However, in line with the SRA for diffuse sky irradiance, partitioning the sky vault is recommended to achieve more realistic results for longwave sky radiation [17]. This approach would enhance air quality and refine estimates of radiant load on humans, thus integrating the concept of anisotropy.

Celestial radiation is composed of three main components: direct shortwave irradiation, diffuse shortwave irradiation, and longwave irradiation. The mean radiant flux used in SOLWEIG is based on the equation developed, which divides the observed global radiation into direct and diffuse shortwaves [18]. The observed global radiation in both direct and diffuse shortwaves is described as follows, with the mean radiant flux (Sstr):

$$S_{str} = \alpha_k \left[0.28K_{\text{dir.side}} + 0.06\left(K_{\text{up}} + K_{\text{down}}\right) + 0.88K_{\text{diff.side}}\right] + \varepsilon_p \left[0.88L_{\text{side.average}} + 0.06\left(L_{\text{up}} + L_{\text{down}}\right)\right]$$

α_k: is the absorption coefficient for short-wave radiation (standard value 0.7)

ε_p : the average emissivity of the human body of the human body (equal to the long-wave absorption coefficient according to Kirchoff's law, with a standard value of 0.97, set here at 0.9).

K_(dir.side) : is the horizontal component of direct radiation normal to the surface of the cylinder body.

K_(diff.side) : the corresponding diffuse radiation. L_(side. average) : average flux of the four cardinal points of the long-wave sensors. The coefficients 0.28, 0.06 and 0.88 are cylinder form factors. Vertical section area, top/bottom, and bole area.

K_up : outgoing radiation. L_up : short-wave radiation emitted from above.

K_down : short-wave radiation from high output. L_down broad-wavelength radiation emitted from above

In SOLWEIG, expression is used to estimate global clear-sky emissivity (εsky): (isotropic case) [16]:

$$\varepsilon_{\text{sky}} = 1 - \left(1 + 46.5\frac{e_a}{T_a}\right) \bullet \exp\left(-\left(1.2 + 3.0 \bullet 46.5\frac{e_a}{T_a}\right)^{0.5}\right)$$

Where Ta is the air temperature at standard height (2 m) and e_a is the actual vapor pressure in hPa calculated from observations of relative humidity at standard height, where e_a in SOLWEIG is estimated from Ta and relative humidity (RH):

$$T_{mrt} = \sqrt[4]{\left(\frac{S_{str}}{\varepsilon_p \sigma}\right)} - 273.15$$

2.4. Simulation Parameters

Meteorological data, along with raster data containing information on building and ground elevation (DSM) and relative humidity, were sourced from a compiled dataset. Ground cover information, which allows for the differentiation of emissivity, albedo, and surface temperature across various surfaces (e.g., pavement, asphalt, soil, grass), was also included. The mean radiant temperature (MRT) is then calculated for a human, modeled as either a box or a cylinder.

3. Results

3.1. Study Zones

The calculation models for the (MRT) simulation were carried out for 4 zones with different characteristics, selected according to the criteria in Table 1 below:

Climate Local Zone CLZ	Central zone Z1	Natural Park zone Z2	Peri-urban zone Z3	Rural zone Z4	
Morphology	Ratio surface 1 / typology	Building +++++	Canopy +++++	Building +++	Canopy +++++
	Ratio surface 2 / typology	Bitumen +++ Other +	Land +++ Other +	Land +++ Other +	Land +++++ Other +
Geometry	Heights	LH	HH	MH	LH
	Density / Occupation	Medium	High	Low	Low
	Orientations	North-South	North-South	North-South	North-South
	Opacity / glazing ratio	Mean/ 0.3	High /na	Low/ na	Low/ na
	Inertia	Medium	Low	Low	Low
Material properties	Lateral Emissivity	0.91	0.71	0.91	0.71
	Ground Emissivity	0.95	0.71	0.85	0.71
	Lateral Albedo	0.25	0.2	0.25	0.2
	Ground Albedo	0.2	0.11	0.15	0.11

Atmospheric properties	Radiative absorption SW/ LW	0.7/0.95***			
	Shading	Integrated according to sky view factor SVF			
	Sky view factor SKV	0.5-0.7	<0.4	>0.7	>0.9
	Meteorological data (RH%, Air T ...)	EPW Meteorological database			

Table 1: Criteria for Selecting Study Areas

References table 1:

Surface ratio 1: surface Digital surface model _ (wall+ roof) / Surface ratio 2: normalized digital surface model (net floor area)

MH: Medium Height / LH: Low Height / HH: High Height / na: not applicable

Glazed area ratio (0.3/ 30% glazed area) / Opacity: degree of light penetration at urban ground level.

SKV (sky view factor): Ratio between the part of the sky hemisphere visible from the ground and that of an unobstructed hemisphere.

*** radiative absorption value with non-absorbent atmosphere option.

+++++: dominant surface / +++: surface with medium representativeness and +: low representativeness

The different study zones are presented as follows:

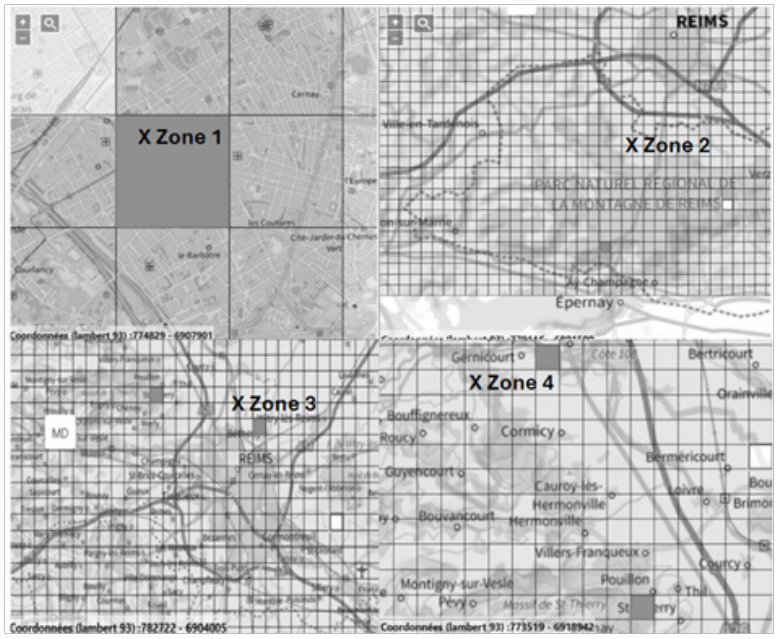

Figure 8: Geographical Map of Study Areas Source: LiDAR HD | Géoservices (ign.fr)

To develop the various simulations of mean radiant temperature, Table 2 below presents the calculation conditions, distinguishing between variable data specific to each zone and fixed calculation parameters applicable to all zones:

Zones	Central zone _Z1	Natural Park zone Z2	Peri-urban zone Bétheny Z3	Rural Zone Z4
Variable data for different zones				

Mean ground emissivity	0,95	0,71	0,85	0,71
Mean ground albedo	0,2	0,11	0,15	0,11
Mean lateral emissivity	0,91	0,71	0,91	0,71
Mean lateral albedo	0,25	0,2	0,25	0,2
Fixed data				
Short- wavelength absorptivity 0.70	0.70			
Wide-wavelength absorptivity	0.95			
Body position	Standing			
Age/weight/ height/height measurement	35ans /75 kg /1.8m /1.8 m			
Clothing	0.9 clo			
Activity	60w			
Meteorological data	Values for direct, diffuse and global shortwave radiation, air temperature and relative humidity are based on ESRI EPW DATA meteorological data for the study area in the city of Reims, France.			

Table 2: Variable and Fixed Conditions for Calculating the Radiative Properties of the Various Study Zones

Reference Table 2:

***Emissivity value between 0 and 1 gray body.**

****Average value based on satellite observation of albedo in the visible and infrared.**

3.2. Results of Mean Radiative Temperature (MRT) Analysis on Study Zones

The mean radiant temperature (MRT) calculations, simulated using the UMEP (Urban Multi-scale Environmental Predictor) and SOLWEIG (Solar and LongWave Environmental Irradiance Geometry) models, were conducted for the reference year 2013, spanning 365 days. The simulations utilized an EPW meteorological database source EPW Map (ladybug.tools), which was directly integrated into SOLWEIG. To analyze MRT across the study zones, a 24-hour analysis was performed on two specific days: D10 (January 10) and D203 (July 22), as illustrated in Figures 9 and 10 below.

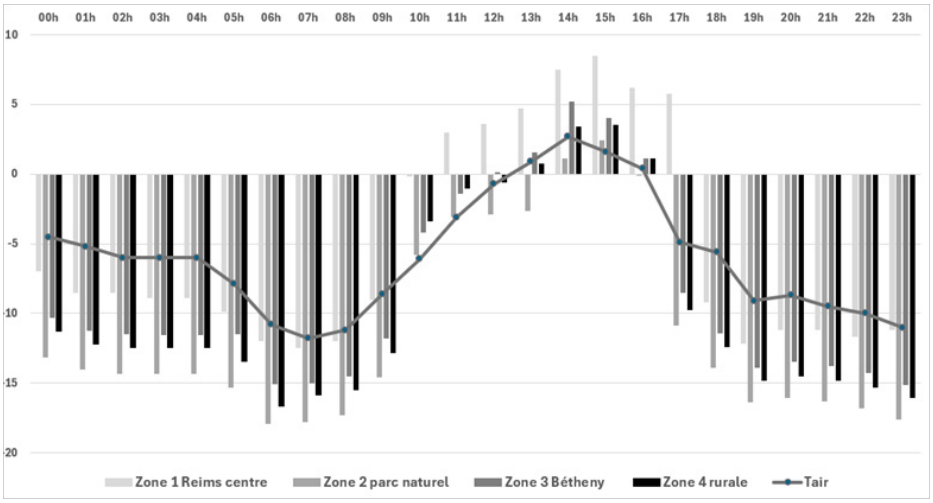

Figure 9: Analysis of the mean Radiative Temperature of the Study Areas Over 24 hours in January as a Function of Air Temperature

Figure 9 illustrates the hourly evolution of temperature differences across four areas surrounding Reims (city center, natural park, Bétheny, rural zone). A typical winter thermal pattern is observed: temperatures drop sharply during the night, reaching a minimum around 7–8 a.m., then rise again during the day until approximately 3 p.m. Rural areas exhibit the lowest temperatures, especially at night, whereas the city center remains significantly warmer, indicating the presence of an urban heat island effect. This thermal contrast between urban and rural zones highlights the impact of urbanization on local climate conditions, particularly with respect to nocturnal cooling.

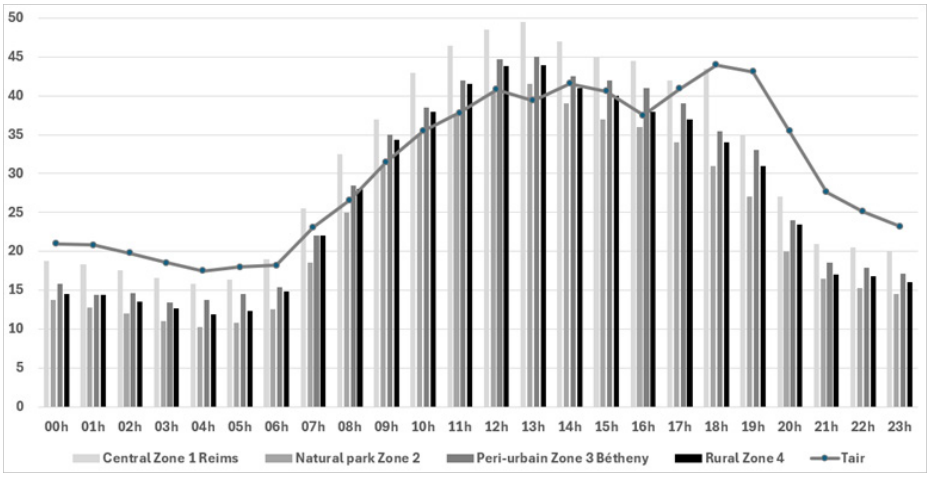

Figure 10: Analysis of the Mean Radiative Temperature of the study Areas Over 24 hours in July as a Function of Air Temperature

Figure 10 highlights the major influence of surface type (urban vs. natural) on daytime heating. The city center accumulates more heat and releases it more slowly, thereby intensifying the urban heat island effect through elevated mean radiant temperature, particularly in the late afternoon. In contrast, vegetated or rural areas respond more rapidly to changes in solar exposure and remain comparatively cooler.

For both analyzed seasons, the mean radiant temperature (MRT) shows strong sensitivity to air temperature in Zone 1 (Reims city center). This sensitivity is attributed to increased radiative flux exchanges in all six directions (horizontal and vertical) with the numerous surrounding urban surfaces. In contrast, MRT is significantly less affected by air temperature in the rural zone, due to the low density of reflective or emissive surfaces, which limits radiative exchanges.

The average MRT difference between the city center and the rural zone reaches 4 °C in winter (D10) and up to 5 °C in summer (D203). This is explained by variations in urban morphology and radiative properties (emissivity and albedo) specific to each zone. Furthermore, MRT is lowest in the natural park area, suggesting that a low albedo, combined with vegetation cover, effectively contributes to reducing surface radiative heating.

Urban geometry, particularly the orientation and height of buildings, also plays a significant role in variations in radiative temperature. For instance, in central Reims, a temperature difference of up to 7°C was observed between north- and south-facing orientations of buildings, even when they share identical radiative properties (Figure 11 below).

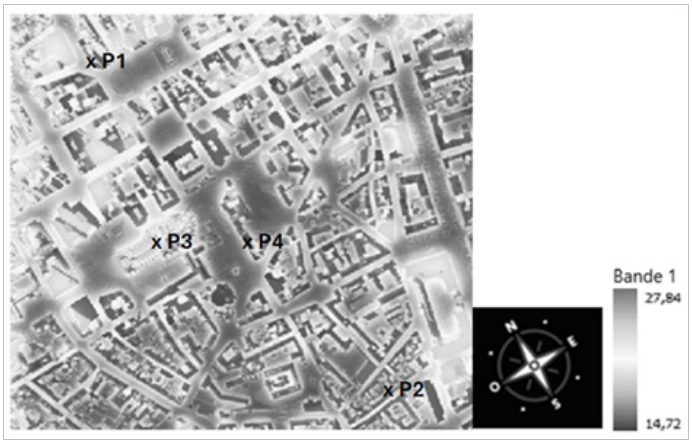

Figure 11: Mean Radiative Temperature at Various Measurement Points as a Function of Orientation and Height at the Center of Reims in July at 9:00 pm

It was also observed in the mean radiative temperature (MRT) simulation calculations that shading has a significant impact on (MRT) in the summer period, figure 12 below:

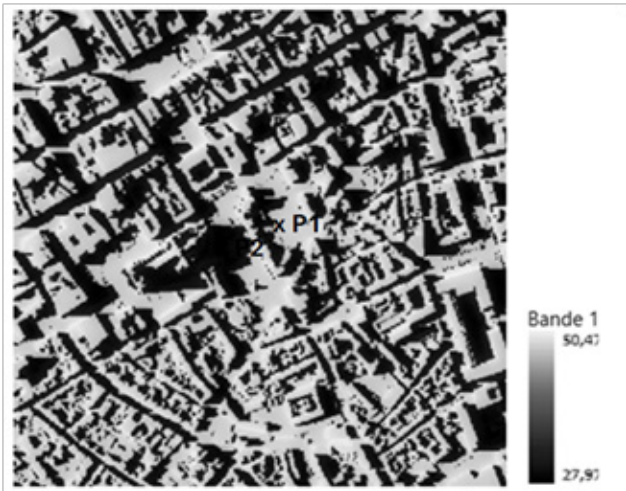

Figure12: Mean Radiative Temperature at Various Measurement Points in Relation to Shading at the Center of Reims in July at 6:00 p.m

3.3. Mean Radiative Temperature (MRT) Optimization Scenarios

The development of mean radiant temperature (MRT) scenarios involves integrating climate change projections and the impacts of urban development to anticipate future thermal conditions. In this study, we propose scenarios aimed at optimizing surface emissivity and albedo, drawing on emissivity data for grey body materials and satellite-derived albedo measurements in both the visible and infrared spectra.

Zone 1	Emissivity mean_soil	Emissivity mean_ Lateral	Albedo mean_ soil	Albedo mean_ Lateral	Soil References proprieties	lateral References proprieties
Reference	0,95	0,91	0,2	0,25	Dry soil	Solid concrete
Scenario 1	0,93	0,89	0,19	0,23	Asphalt/bitumen	
Scenario 2	0,91	0,87	0,18	0,21	Solid/reinforced concrete	Glazing
Scenario 3	0,89	0,85	0,17	0,19		
Scenario 4	0,87	0,83	0,16	0,17		
Scenario 5	0,85	0,81	0,15	0,15		Wood
Scenario 6	0,8	0,79	0,14	0,13	Resign	Acrylic paint
Scenario 7	0,74	0,73	0,11	0,1	Vegetation/ grass	

Table 3: Scenarios for Optimizing Mean Radiative Temperature (MRT)

Average soil and lateral emissivity: wavelength-independent grey body	from 0 to 1
Short-wave absorptivity	0,7
Long-wave absorptivity	0,95
The average emissivity of the human body (equal to the long-wave absorption coefficient according to Kirchhoff's law with a standard value of 0.97, set here at.	0,9
Average soil and lateral albedo	from 0.1 to 0.25

Table 4: Simulation Condition

Improving mean radiant temperature (MRT) can be achieved through the optimization of surface emissivity and albedo, as illustrated in Figures 13 and 14. Based on satellite observations, surfaces with lower albedo absorb less visible radiation from the sky, thereby reducing the temperature of both ground and vertical surfaces. This limits the emission of short- and long-wave infrared radiation and consequently contributes to lowering MRT.

To explore this optimization, seven scenarios were developed, including a reference scenario. The results indicate that beyond Scenario 5 (mean soil emissivity: 0.85, mean soil albedo: 0.15; mean lateral emissivity: 0.81, mean lateral albedo: 0.15), MRT drops significantly in winter, leading to potential thermal discomfort during the colder months—despite the continued decrease in MRT during summer.
Scenario 3 (mean soil emissivity: 0.89, mean soil albedo: 0.17; mean lateral emissivity: 0.85, mean lateral albedo: 0.19), as shown in Figure 14, offers a balanced solution across both winter and summer conditions. Compared to the reference scenario (mean soil emissivity: 0.95, mean soil albedo: 0.20; mean lateral emissivity: 0.91, mean lateral albedo: 0.25), this scenario enables an effective compromise between outdoor thermal comfort and the energy demands associated with building heating and cooling.

The impact of material radiative properties (albedo and emissivity) on mean radiant temperature (MRT), as assessed through seven simulation scenarios compared to a reference case, demonstrates that reducing albedo leads to lower absorption of incoming visible radiation, thereby decreasing surface temperatures—particularly on lateral and ground surfaces. This results in a reduction of MRT, which translates into improved thermal comfort during the summer period. However, from scenario 5 onward, this reduction becomes problematic in winter, as MRT drops excessively, posing a risk of thermal discomfort. Scenario 3 emerges as the optimal compromise, balancing summer and winter comfort by moderately adjusting albedo and emissivity. These simulations highlight the importance of finely tuning the radiative and optical properties of urban materials to achieve seasonally balanced thermal performance.

Figure 13 below illustrates the impact of various albedo and emissivity modification scenarios on winter MRT. It shows that the more surface properties tend to reflect radiation (i.e., high albedo and low emissivity), the more MRT decreases, potentially causing winter thermal discomfort. Scenarios 5 through 7 display the lowest MRT values, while scenario 3 offers a balanced outcome—slightly reducing MRT compared to the reference without inducing excessive cooling. Thus, this scenario appears to be the most suitable for preserving thermal comfort in urban environments during winter.

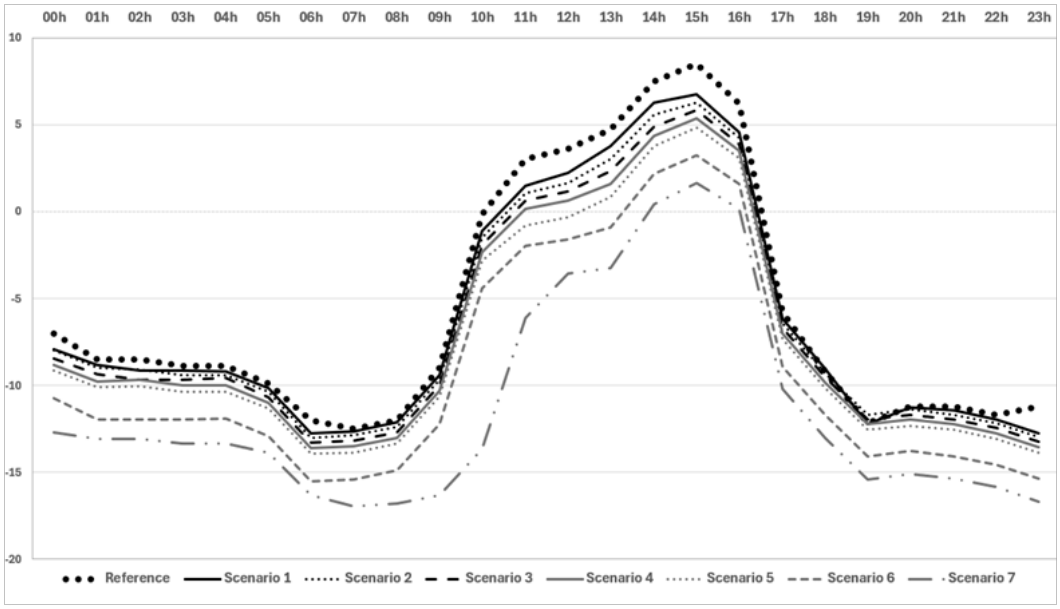

Figure13: Evolution of Mean Radiative Temperature as a Function of Different Scenarios for Optimizing Emissivity and Albedo over 24 hours in January

Figure 14 highlights the importance of optimized management of urban surface radiative properties to reduce thermal exposure during summer. Scenarios incorporating more reflective surfaces (high albedo) or surfaces with lower emissivity effectively reduce mean radiant temperature (MRT) by up to 10 °C on average during critical hours. However, excessive optimization may lead to thermal discomfort during winter. Therefore, Scenario 3 appears to offer the most balanced approach, providing effective thermal attenuation in summer while remaining compatible with winter comfort requirements.

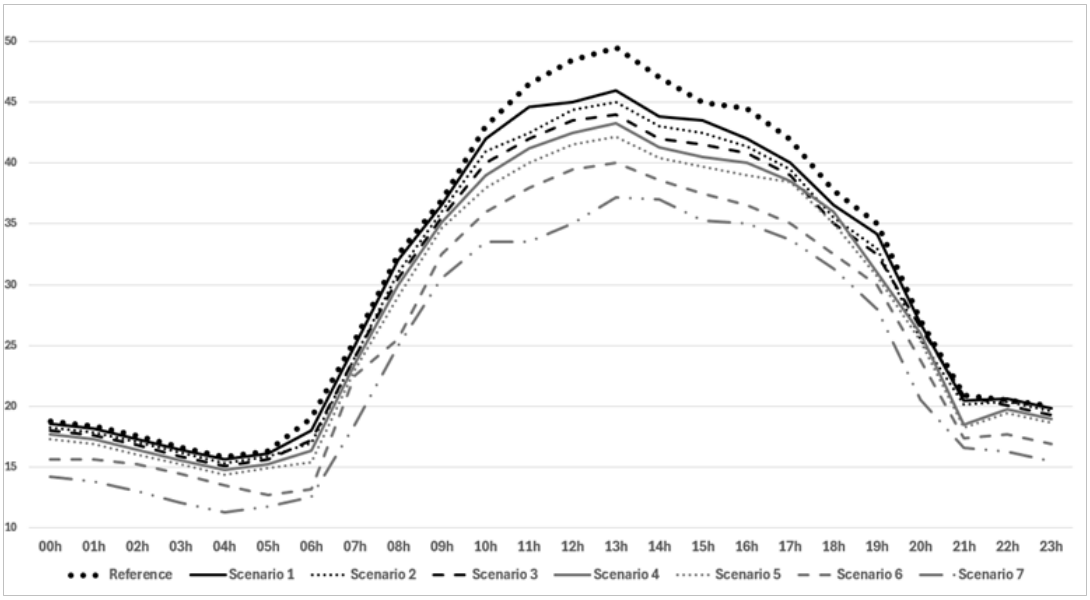

Figure14: Evolution of Mean Radiative Temperature as a Function of Different Scenarios for Optimizing Emissivity and Albedo Over a 24-hour day in July

In the context of climate warming and increasing urbanization, mitigating summer temperatures has become a priority to reduce health and energy risks associated with heatwaves. However, maintaining seasonal balance is essential, as strategies that are effective in summer (such as high-albedo surfaces) can lead to excessive cooling in winter, resulting in thermal discomfort and increased heating demand.

Therefore, the optimal approach is to prioritize summer mitigation while adjusting radiative properties in a way that does not negatively impact winter conditions. Scenario 3 illustrates this well, offering a seasonally balanced thermal regulation strategy.

Figure 15 below illustrates the differences in mean radiant temperature (MRT) across the various scenarios compared to the reference case, with the lower section representing winter conditions and the upper section representing summer conditions

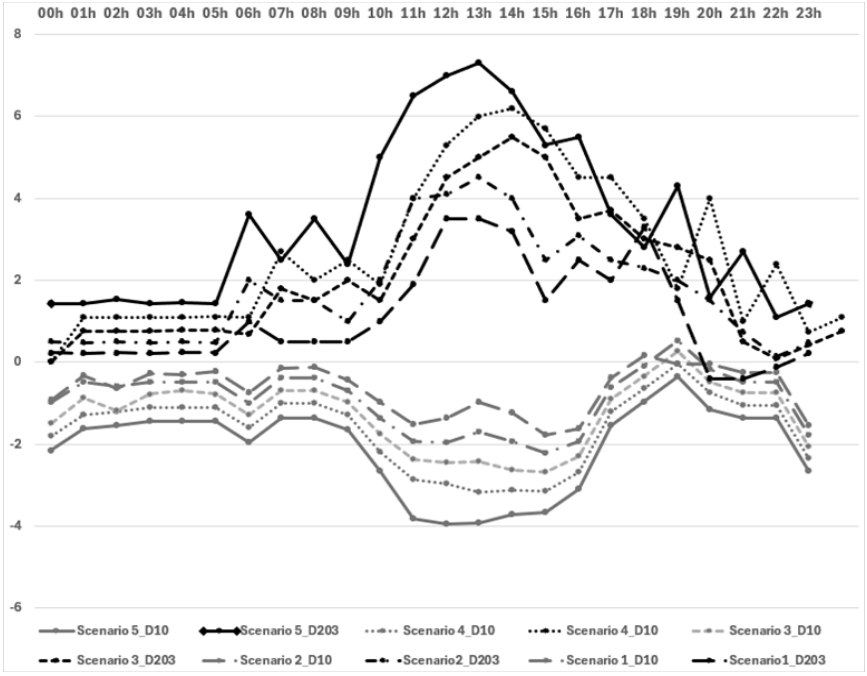

Figure 15: Difference in Mean Radiative Temperature (MRT) between the First 5 Optimization Scenarios Compared with the Baseline

This graph highlights the potential of urban radiative modifications (albedo, emissivity) to reduce summer mean radiant temperature and improve urban thermal comfort. It suggests that balanced scenarios (such as scenarios 3 or 4) could provide an effective compromise between summer performance and the preservation of winter comfort.

The mean radiant temperature (MRT) is more sensitive to irradiation from the lower sky and ground surfaces than to lateral longwave infrared emissions from building façades, Figure 16 illustrates the sensitivity of MRT to varying values of soil and lateral surface emissivity.

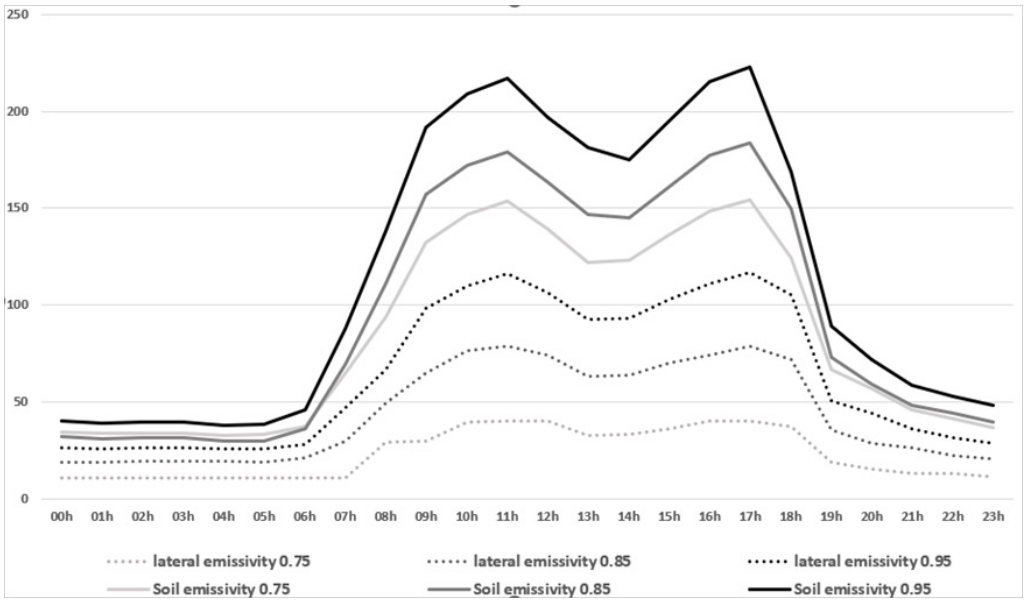

Figure 16: Analysis of the Sensitivity of Mean Radiative Temperature to Variations in wall and Ground Emissivities in the Central Area of Reims

This graph illustrates the importance and sensitivity of radiative emissivity in the daily thermal dynamics of urban heat islands. An increase in horizontal ground emissivity has a more pronounced effect than that of vertical surfaces, significantly amplifying daily temperature variations, with sharper peaks during the day. This behavior is driven by factors such as orientation and exposure to solar radiation, thermal capacity and inertia, emission angle and view factor effects, as well as surface properties and roughness. These findings highlight the critical role of material selection and the radiative properties of surface coatings in thermal management strategies.

4. Conclusions

Mean radiant temperature (MRT) is significantly influenced by surface albedo and emissivity. A reduction in these two parameters leads to decreased absorption of incoming longwave and visible radiation from the sky, as well as diminished re-emission of thermal energy in the longwave infrared and visible spectra. Across the study zones, MRT tends to follow the diurnal pattern of air temperature. However, notable deviations are observed in Zone 1, where urban surfaces are exposed to extreme temperatures and direct solar radiation, particularly during midday hours.

The increased sensitivity of the ground to emissivity can be explained by several physical factors. Firstly, due to its horizontal orientation, the ground receives more intense and prolonged direct solar radiation compared to vertical or inclined surfaces, which amplifies its heating. Secondly, its high thermal capacity allows it to store and release greater amounts of energy, thereby enhancing the effect of emissivity on surface temperature. Furthermore, emissivity depends on shape factors and emission angles; horizontal surfaces exhibit a more significant directional distribution of radiation in the overall thermal balance. Additionally, the roughness of the ground, often greater than that of urban facades, increases the hemispherical emissivity, making the ground more sensitive to radiative variations and directly impacting the mean radiant temperature (MRT) [19-22].

High-albedo and low-emissivity scenarios effectively reduce the mean radiant temperature (MRT) during the daytime, thereby limiting summer thermal stress. However, they can intensify nocturnal cooling, which is beneficial in summer but problematic in winter. A reduction in MRT is particularly important in dense urban environments to mitigate heat islands and decrease cooling demand. Intermediate scenarios, such as scenarios 3 or 4, provide a good compromise by maintaining a moderate MRT both day and night, thus ensuring a thermal balance between seasons.

MRT plays a central role in the assessment of thermal comfort and radiative exchanges in urban environments. It directly affects the perception of heat within urban heat islands (UHIs) by representing the net radiative fluxes exchanged among various urban surfaces.

As such, it is a critical parameter for evaluating outdoor thermal comfort and for understanding the mechanisms behind UHI formation, which pose serious challenges in terms of public health, environmental degradation, and increased energy demand.

Incorporating MRT into UHI analysis enables the formulation of targeted strategies to mitigate their adverse effects. As demonstrated by the results in this study, optimizing the radiative properties—specifically, albedo and emissivity—of both ground and vertical surfaces contributes to the reduction of MRT and, consequently, enhances outdoor thermal comfort. Furthermore, findings indicate that MRT is more sensitive to radiation exchanges from horizontal surfaces than from vertical ones. This suggests that prioritizing the thermal refurbishment of ground-level materials is more effective than focusing solely on building façades.

The study also highlights the potential of expanding vegetated areas—particularly in urban parks—as a viable mitigation strategy. Vegetation, characterized by low albedo and high evapotranspiration, can significantly reduce the absorption and re-emission of longwave radiation, as observed in Zone 2. Integrating urban canopies requires preliminary analysis to ensure their optimal placement, considering the dual effect of vegetation: the replacement of sensible heat flux by latent heat flux, and the shading provided by tree cover.

Finally, analyzing MRT across different wavelengths reveals critical insights into the radiative behaviour of the modelled scenarios. It is important to note that greenhouse gas (GHG) emissions further alter these dynamics by disrupting radiative heat transfer processes, thereby amplifying urban heat island effects.

To address these challenges, it is essential to develop mitigation strategies at the urban scale. The results and reflections presented in this article should be integrated into urban planning policies, encouraging the adoption of surface materials and coatings with optimized radiative properties. Such approaches will contribute not only to UHI mitigation but also to broader climate adaptation efforts through the reduction of GHG emissions.

Acknowledgements

This work, carried out as part of a doctoral thesis since 2022 within the Ecole Doctoral Mathematics Physics Digital and Engineering Sciences MPSNI of the University of Reims Champagne Ardenne URCA, has benefited from the excellence and quality of the scientific supervision.

References:

1. GIEC-IPCC : SR15_Summary_Volume_french.pdf
2. Bocquier, P. (2005). World Urbanization Prospects: an alternative to the UN model of projection compatible with the mobility transition theory. *Demographic Research, 12,* 197-236.
3. Stewart, I. D., & Oke, T. R. (2012). Local climate zones for urban temperature studies. *Bulletin of the American Meteorological Society, 93*(12), 1879-1900.
4. Santamouris, M. (2020). Recent progress on urban overheating and heat island research. Integrated assessment of the energy, environmental, vulnerability and health impact. Synergies with the global climate change. *Energy and Buildings, 207*, 109482.
5. Fraisse, P. (2020). Délos: Études de morphologie urbaine I Objectifs et méthodes. *Bulletin de correspondance hellénique*, (144.1).
6. Santamouris, M. (2016). Cooling the buildings–past, present and future. *Energy and Buildings, 128,* 617-638.
7. Mirzabeigi, S., & Razkenari, M. (2022). Design optimization of urban typologies: A framework for evaluating building energy performance and outdoor thermal comfort. *Sustainable Cities and Society, 76*, 103515.
8. Acero, J. A., Koh, E. J., Ruefenacht, L. A., & Norford, L. K. (2021). Modelling the influence of high-rise urban geometry on outdoor thermal comfort in Singapore. *Urban Climate, 36*, 100775.
9. Aghamolaei, R., Fallahpour, M., & Mirzaei, P. A. (2021). Tempo-spatial thermal comfort analysis of urban heat island with coupling of CFD and building energy simulation. *Energy and Buildings, 251*, 111317.
10. Mariani, L., Parisi, S. G., Cola, G., Lafortezza, R., Colangelo, G., & Sanesi, G. (2016). Climatological analysis of the mitigating effect of vegetation on the urban heat island of Milan, Italy. *Science of the Total Environment, 569,* 762-773.
11. Masanori Onishi, Isao Iizawa, Miki Fukuzawa, Satoshi Sakai, Kazuhiro Umetani, Aya Ito, et al., ERAD2010
12. Watson, I. D., & Johnson, G. T. (1987). Graphical estimation of sky view-factors in urban environments. *Journal of climatology, 7*(2), 193-197.
13. Grimmond. (2010). The International Urban Energy Balance Models Comparison Project: First Results from Phase 1 in: Journal of Applied Meteorology and Climatology Volume 49 Issue 6.
14. Lindberg, F., Grimmond, C. S. B., Gabey, A., Huang, B., Kent, C. W., Sun, T., ... & Zhang, Z. (2018). Urban Multi-scale Environmental Predictor (UMEP): An integrated tool for city-based climate services. *Environmental modelling & software, 99,* 70-87.
15. Lindberg, F., Grimmond, C. S. B., Gabey, A., Huang, B., Kent, C. W., Sun, T., ... & Zhang, Z. (2018). Urban Multi-scale Environmental Predictor (UMEP): An integrated tool for city-based climate services. *Environmental modelling & software, 99*, 70-87.
16. Prata, A. J. (1996). A new long-wave formula for estimating downward clear-sky radiation at the surface. *Quarterly Journal of the Royal Meteorological Society, 122*(533), 1127-1151.
17. Robinson, D., & Stone, A. (2004). Solar radiation modelling in the urban context. *Solar energy, 77*(3), 295-309.
18. Holmer et al. (2015). http://www.meteo.fr/cic/meetings/2015/ICUC9/LongAbstracts/bph5-2-3271344_a.pdf
19. Huo, T., Xu, L., Feng, W., Cai, W., & Liu, B. (2021). Dynamic scenario simulations of carbon emission peak in China's city-scale urban residential building sector through 2050. *Energy*

Policy, 159, 112612.
20. Davin, E. L., & de Noblet-Ducoudré, N. (2010). Climatic impact of global-scale deforestation: Radiative versus nonradiative processes. *Journal of Climate, 23*(1), 97-112.
21. Wallenberg, N., Lindberg, F., Holmer, B., & Thorsson, S. (2020). The influence of anisotropic diffuse shortwave radiation on mean radiant temperature in outdoor urban environments. *Urban Climate, 31*, 100589.
22. Unsworth, M. H., & Monteith, J. L. (1975). Long-wave radiation at the ground I. Angular distribution of incoming radiation. *Quarterly Journal of the Royal Meteorological Society, 101*(427), 13-24.